Int. J. Multiphase Flow Vol. 17, No. 1, pp. 103–118, 1991
Printed in Great Britain.

0301-9322/91 $3.00 + 0.00

EXPERIMENTAL INVESTIGATION OF A TURBULENT FILTRATIONAL FLOW

A. R. YEVSEYEV, V. E. NAKORYAKOV and N. N. ROMANOV
Institute of Thermophysics, Siberian Branch of the U.S.S.R. Academy of Sciences, 630090 Novosibirsk-90, U.S.S.R.

(Received 1 September 1989; in revised form 5 June 1990)

Abstract—A filtrational flow in a regular packed bed is arranged so that it allows both direct measurement of the velocity distribution in the layer and flow visualization. Detailed diagrams of mean velocities and the flow turbulence levels, as well as one-dimensional spectra of longitudinal velocity pulsations, have been obtained using LDA for an optically transparent system of glass spheres and a special immersion system. Reynolds numbers, calculated from the sphere diameter and the flow velocity in a minimal cross-section between the spheres, are in the range 1000–20,000.

It has been established that the flow past a regular array of spheres is of jet character. The flow past the contact points of spheres results in a local flow separation, the value of such a separation zone being mainly dependent on the method of sphere packing. On the basis of the experimental results, the turbulence generation mechanism in regular arrays of spheres is presented.

Key Words: filtrational flow, turbulence, LDA, flow past spheres.

1. INTRODUCTION

A considerable number of both experimental and theoretical works, which were initiated in the last century by Darcy's experiments, have been devoted to the investigation of the hydrodynamics of filtrational flows. The integral characteristics of filtrational flow, i.e. the dependence of the pressure drop in a layer on the liquid flow rate as well as on the size, shape and arrangement of the spheres, have been reported by Aerov & Todes (1968), Aerov *et al.* (1972), Bogoyavlenskii (1978) and Gol'dshtik (1984); an extensive bibliography is presented in these works. Both the concept of internal flow, in which an analogy with flow in the system of parallel capillaries is made, and the concept of external flow past the elements of the solid phase are applied for the interpretation of the characteristics of filtrational flow.

The detailed study of the hydrodynamic characteristics of filtrational flow at the level of pores is needed to obtain greater insight into the physics of the process at Reynolds numbers (Re) which are significantly larger than unity. The investigation of dye motion along a sphere surface in a rhombohedral arrangement of Plexiglas was carried out by Wegner *et al.* (1971) in a system where the refractive indices of the liquid and spheres were close. A stable flow was observed, at $Re = 82$, which had distinct regions of flow reversing on the sphere surface. The flow pattern was preserved when Re increased up to 200, where the laminar flow became unstable. Flow separation near the sphere surface into different zones took place at contact points between the spheres at $Re > 40$. All the flow separation regions are behind the contact points of the spheres. In a shadow zone of the sphere, the last four separated regions merge downstream to form a single separation zone.

In an earlier work, Jolls & Hanratty (1966) studied the effects of Re on local velocity gradients and local mass transfer rates on a packing surface, and concluded that the flow over most of the surface can be described by the three-dimensional boundary layer equation at $Re > 40$. The flow was found to be more sensitive to the packing and, particularly, to the arrangement of contact points than to flow velocity variations. The critical Re range for filtration flow was found to be 110–150.

Local velocity gradients and pressure distribution over a sphere surface in a rhombohedrally packed array of spheres and in a single layer of spheres were measured by Karabelas *et al.* (1973). Measurements and visualization of the flow around a sphere in a layer of spheres suggested a particular effect of contact points over the Re range 50–1200. A model of streamlines near the

surface and the region of flow separation from the sphere, which varies along a longitudinal coordinate from 110 to 135° was developed on the basis of the visual studies. The results, obtained for a rhombohedrically packed array of spheres, including local mass transfer measurements, had been interpreted in terms of visual studies previously by the authors (Wegner *et al.* 1971). On the basis of the above experiments, a model of filtrational flow at the surface of a sphere was suggested for varying Re. Visual investigations of filtrational flow in a chaotic glass bead arrangement in the Re range 20–1000 have been presented by Kirillov *et al.* (1972). The flow pattern is characterized by joining and dividing jets and a nonflowing portion located in the vicinity of the sphere contact points.

The method of optical homogeneity, by which the refractive indices of the glass spheres and filtrating liquid are matched to a high accuracy, was used for the first time by Johnston *et al.* (1975) for measuring the profile of longitudinal velocity with LDA techniques at $\mathrm{Re} < 1$.

LDA measurements of the longitudinal velocity profiles inside the pores of a filtrational flow in cubic and random arrays of spheres were made by Volkov *et al.* (1980). The refractive indices of the glass spheres and the special immersion liquid were also matched to a high accuracy; up to $\mathrm{Re} = 2000$.

The present paper is an extension of the work by Volkov *et al.* (1980). The aim of the experiments was to obtain a qualitative picture and quantitative characterization of filtrational flow through regular packed beds in the turbulent regime. Re values, determined on the basis of sphere diameter and the flow velocity in the section with the minimum area, varied from 1000 to 20,000.

2. EQUIPMENT AND PROCEDURE

The experimental setup is a closed hydrodynamic loop containing a test section, pump, rotameter, heat exchanger, regulating valve and a pressure tank. The test area is a rectangular channel with dimensions $3D \times 5D$, where $D = 18$ mm is the bead diameter. The lateral walls of the channel were made of optical glass. Fourteen bead layers were placed into a 255 mm high test area. Measurements were performed at the seventh layer. At the test area inlet, a honeycomb was used to make the flow uniform and a thermocouple was employed for temperature control. Thermostabilization of the immersion liquid was carried out in a special refrigerator which uses water circulation.

An aqueous solution of iodine and rhodane ammonium developed by Yevseyev & Ryashentseva (1986) was used as the immersion liquid. The kinematic viscosity of the liquid is nearly the same as that of water, but the density is higher ($\rho = 1.3$ g/cm^3).

The hydrodynamic properties of the flow within the optically transparent system of beads and immersion liquid were measured using the LADO-2 laser-Doppler anemometer, developed through a joint venture by the Institute of Automation and Electrometry, Siberian Branch of the U.S.S.R. Academy of Sciences, and the Karl Zeiss Jena Co. (G.D.R.). The LADO-2 was operated in the forward scattering mode. Typical dimensions of the measuring volume were 100×30 μm. By using a precision traversing mechanism, the measuring volume was traversed over the investigated area of filtration flow.

The refractive indices of the LK-7 optical glass ($n = 1.483$) and the immersion liquid were matched to an accuracy of 10^{-3}, as discussed by Bernard *et al.* (1981). The coordinate was set to within 0.01 mm, the measurement accuracy for the mean velocity was 0.3–0.5% and for the fluctuation velocity, within a band of 500 Hz, was 3%. Doppler signals with the above accuracy were processed by a special tracking processor designed by the Institute of Thermophysics, Siberian Branch of the U.S.S.R. Academy of Sciences. Spectral properties of the fluctuating velocity were measured by a spectroanalyser manufactured by the Brüel & Kjoer Co.

Two types of regular packed beds were used in the experiments: a cubic arrangement with through channels and an average volumetric porosity of 0.476; and an octahedric arrangement with blocked channels and a porosity of 0.2595. The geometric parameters of the bed, cells, channel cross-section variations inside them (Borishanskii 1958) and typical measurement directions are shown in figures 1(a–c); wherein h is the height of a bead cell, ϵ is the volumetric porosity and x, y and z are the cartesian coordinates, with the z-axis in the downstream direction.

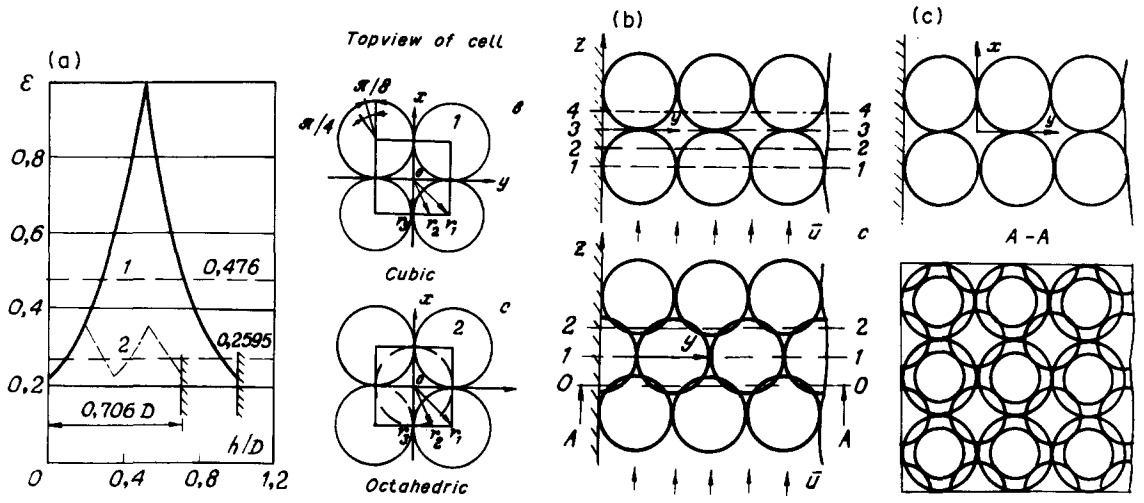

Figure 1. Porosity distribution and basic measurement directions inside a bead cell (a), a cubic cell (b) and an octahedric cell (c).

Taking into account the flow symmetry in an elementary cell, measurements were performed in the following directions: r_1—at an angle of $\pi/4$ to the x-axis; r_2—at an angle of $\pi/8$ to the x-axis; r_3—in the direction of the x-axis and also along the y-axis. Additional measurements were performed for a near-wall cell, i.e. a cell adjacent to the channel wall, along the x-axis with a spacing of 1.5 mm. Measurements were carried out downstream (the z-axis) in four sections located at a spacing of $D/4$ apart.

In a cell of a maximally dense octahedric packed bed, measurement sections z_0, z_1, and z_2 go through four contact points of the beads. The coordinate axes xy in sections z_0 and z_2 are positioned at an angle of $\pi/4$ in relation to the initial position of the cell.

Velocity vector projections are denoted by the coordinate axes: $Z \leftrightarrow u$, $y \leftrightarrow v$, $x \leftrightarrow w$. An overbar designates a time-averaged velocity and a prime indicates a fluctuating velocity.

3. FILTRATION PROCESSES IN A CUBIC PACKED BED

Investigations on the local flow structure in the near-wall and central cells using the coordinate grid described above yielded extensive experimental information.

The sphere diameter D and maximum velocity U_m in the cell are taken as length and velocity scales.

The flow character inside the layer at $\mathrm{Re} = 1000$ is shown in figures 2(a,b). The visual studies of the flow were carried out using small air bubbles. A laser knife was used to illuminate the flow in a given plane. The whole velocity field may be divided into equal cells. In the wake region of the spheres, separation zones, with sizes comparable to the sphere diameter, are clearly seen. In a cubic packed bed, the jets flowing in the through channels have a velocity much higher than that in the separation zones. The return flow structure in the wake zone of the sphere is illustrated in figure 2(b). The visual pattern of the flow corresponds to a plane at a distance of $y/D = 1.085$ from a wide wall of the channel.

Figures 3(a, b) show the dimensionless profiles of the longitudinal velocity, $\bar{u}/\bar{u}_m$, and r.m.s. fluctuating velocities, $\sqrt{\overline{u'^2}}/\bar{u}_m$, in the zy symmetry plane (at $x = 0$) for the central and near-wall cells at $\mathrm{Re} = 1.74 \cdot 10^4$. Profile 1 was measured in the section, $y/D = 0$, which has the minimum flow area. It consists of a near-wall jet ($y/D = 0$ to 0.5) and a central jet ($y/D = 0.5$ to 1.5). A velocity maximum is located in the geometric centre of the cell and minima of zero are found at the lateral channel wall and contact points. Near the indicated contact points the velocity profile has an inflection. Turbulence in this region has a maximum value of 24%. Near the channel wall a second maximum in the fluctuating velocity is associated with turbulence generation. In other parts of the jet the turbulence level is 5–7%.

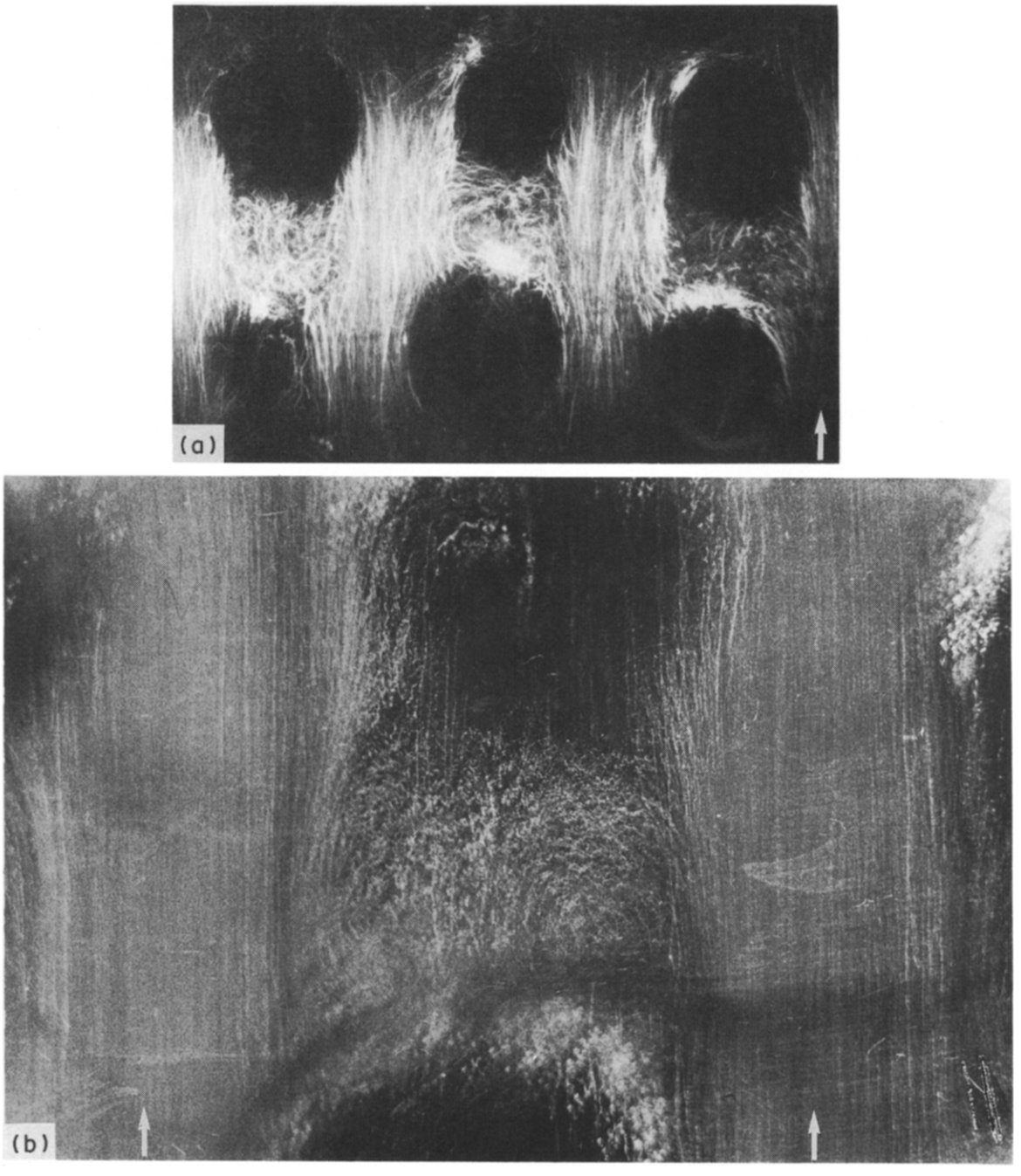

Figures 2(a, b). Turbulent filtrational flow in a cubic array of spheres (a); close shot (b) in the zx plane ($y/D = 1.085$, Re = 1000).

Profile 2, in a diverging region ($h/D = 0.25$), has an area of negative velocity located behind the contact points. The negative velocity here is minus $(0.1–0.2)\cdot u_m$ and the turbulence level is $\sim 5\%$. In the middle of each cell the flow is a jet, formed in the previous section (1). Between the jet and the reverse flow part one can single out a transition area (a mixing layer) with a maximum fluctuating velocity of 24%. The velocity profile in the central jet has a small local minimum at the cell longitudinal symmetry axis, where the velocity is $0.8\cdot\bar{u}_m$. The turbulence level in the jets is 12–14%.

Cross-section 3 ($h/D = 0.5$) has the maximum flow area. The velocity profile is qualitatively the same as in cross-section 2. The reverse flow part is located behind the contact points and its extent in the direction of the y-axis is similar to that in the previous section ($\sim 0.3D$). Negative velocities

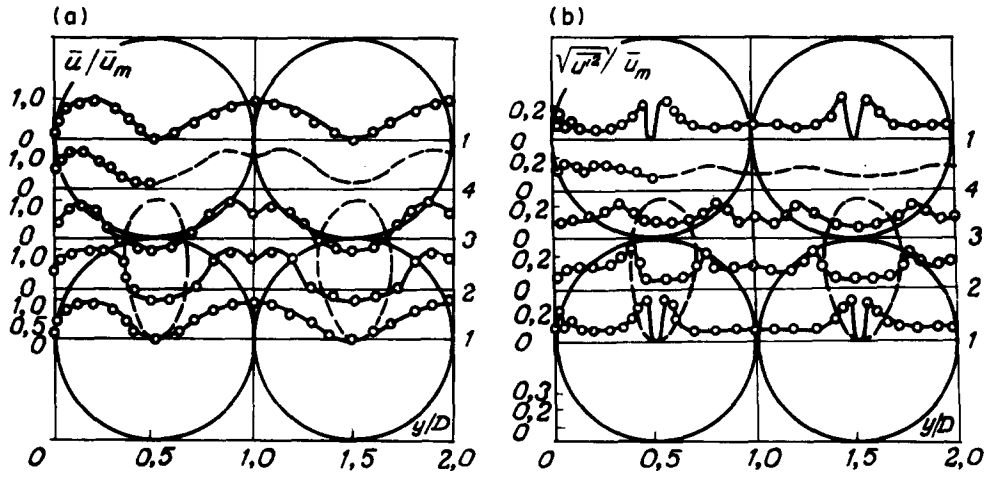

Figures 3(a, b). Profiles for the longitudinal velocity (a) and r.m.s. fluctuations (b) in a cubic cell at $\mathrm{Re} = 1.74 \cdot 10^4$ in the zx plane (at $y/D = 0$).

in this part are about $0.2 \cdot \bar{U}_m$ and the turbulence level increases up to $\sim 10\%$. In the jet part, the turbulence level is $\sim 12\%$. In the mixing layer betwen two counter-flows the velocity profile has inflection points and the turbulence is close to a maximum level of 20%.

The velocity diagram for the converging section 4 ($h/D = 0.75$) is constructed from measurements only in the near-wall cell. The velocity profile 4 is qualitatively similar to that in sections 2 and 3. However, there is no reverse flow here. The velocity minimum behind the contact points equals $0.2 \cdot \bar{U}_m$ and the maximum in the jet part is 1. The flow accelerates while passing through a section with decreasing area, and the velocity fluctuations decrease. The turbulence level varies in a wave-like fashion from 10 to 15%. A local maximum of fluctuations (18%) near the wall is again associated with turbulence generation by the wall. Further downstream the flow returns to its initial state, i.e. as in section 1.

The dashed line in figures 3(a,b) indicates zero velocities separating the reverse flow part and the jet part. The reverse flow areas are evidently formed behind the contact points. Their dimension along the flow is $\sim(0.6\text{–}0.7) \cdot D$, and across the flow $\sim(0.3\text{–}0.4) \cdot D$.

The results show that there are no major differences between the flow patterns in near-wall and central cells in the section under study. The only exception is a region, ~ 1 mm, which is associated with turbulence generation by the channel wall and liquid adhesion to it.

Let us now consider flow around beads within the near-wall cell in the zx planes parallel to the channel wall and located at different distance from it, $y/D = 0.055$ to 0.44. As the distance from the contact points of the beads and the channel wall increases, the bead cross-sectional area also increases; hence the flow area diminishes.

Figures 4(a, b) are diagrams of the mean velocity and turbulence levels at $\mathrm{Re} = 1.74 \cdot 10^4$ in the zx plane at $y/D = 0.055$, located at a distance of 1 mm from the channel wall. The dashed lines denote zero velocity separating the reverse flow part from the main part of the flow. Behind the contact points of the beads with the channel wall reverse flow areas are formed [as in figures 3(a, b)], with downstream lengths of $\sim(0.6\text{–}0.7) \cdot D$ and spanwise lengths of $\sim(0.3\text{–}0.4) \cdot D$. Negative velocities up to $0.2 \cdot \bar{u}_m$ are found in sections 2 and 3 and the turbulence level is $\sim 5\%$. The velocity maximum in the near-wall jets for these sections is $(0.6\text{–}0.7) \cdot \bar{u}_m$ at the cell symmetry axis and the turbulence level is 12–14%. In the transition region between the reverse flow part and the near-wall jets, the velocity fluctuations are much smaller than in figures 3(a,b). The maximum turbulence level increases from 13% in section 1 to 20% in section 3.

A different flow pattern is observed [figures 5(a,b)] in the plane at a distance of $y/D = 0.125$ from the channel wall. The velocity profile is jet-like through the whole cell, in each of its sections. The velocity maximum is located at the symmetry axis in all sections and reaches 1.0 in all sections except section 3. The velocity maximum in the latter section is $0.85 \cdot \bar{u}_m$ and in the area of the wake contact point there is a small region with negative velocities ($\sim 0.1 \cdot \bar{u}_m$). Thus, velocity profiles show

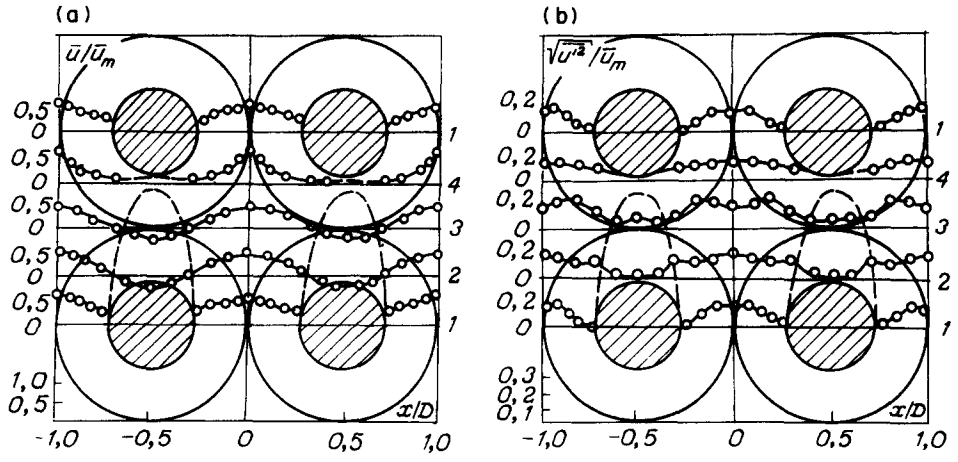

Figures 4(a, b). Profiles for the longitudinal velocity (a) and r.m.s. fluctuations (b) in a cubic cell at $Re = 1.74 \cdot 10^4$ in the zx plane (at $y/D = 0.055$).

that the bead surface is streamlined without separation in the plane under consideration, except for a small zone near the wake contact point. The turbulence level is rather uniform, about 12%, with the exception of two local maxima of 18% in section 3.

The flow patterns in the zx planes of a bead cell at $y/D = 0.222$ and 0.333 are qualitatively similar to that in figures 5(a,b). Most of the bead surface is streamlined without separation. A local separation zone may be singled out only in section 3, near a wake contact point of the beads. The mean velocity decreases in the neighbourhood of the contact point, and the negative velocity zone increases in size. The turbulence level increases from 5% in section 1 to 21% in section 2, and then decreases to, approximately, 10% in sections 3 and 4.

Close to the bead contact points ($y/D = 0.39$), the longitudinal velocity decreases considerably in all cell sections. Velocities close to zero in practically all cell sections have been recorded in the zx plane at $y/D = 0.44$ [figures 6(a,b)]. Gaps for flow between the beads are rather small and the hydrodynamic drag is high. Liquid moves in an oscillatory fashion at nearly zero mean velocity. A maximum turbulence level of 20% is observed now in section 1. In other cell sections, the mean turbulence level is $\sim 12\%$. Near wake contact points in section 3 the turbulence level decreases to 5%.

Consider the flow within the central bead cell in the plane located at an angle of $\pi/4$ in relation to the zr_1 plane. Profiles of the longitudinal velocities in sections 1–3 of the cell indicate a jet-like character of the flow near the beads [figures 7(a, b)]. The dimensionless velocity at the jet axis

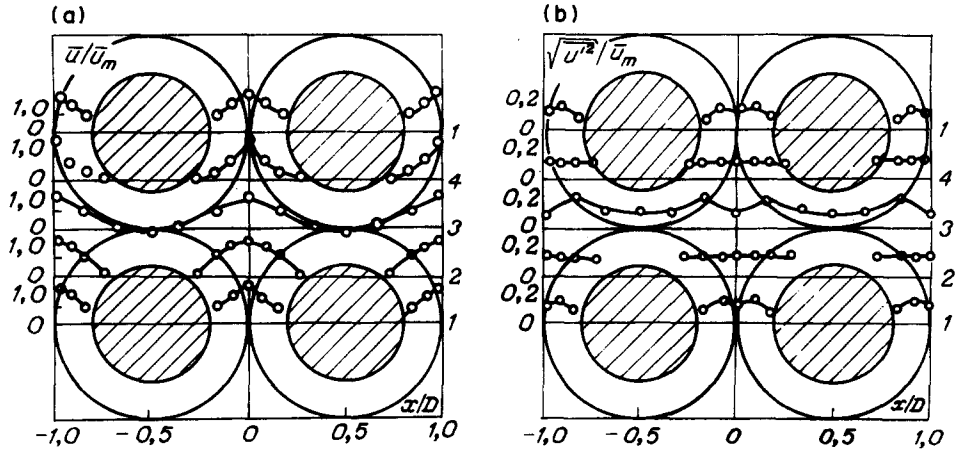

Figures 5(a, b). Longitudinal velocity profiles (a) and turbulent fluctuation levels (b) in a cubic cell at $Re = 1.74 \cdot 10^4$ in the zx plane (at $y/D = 0.125$).

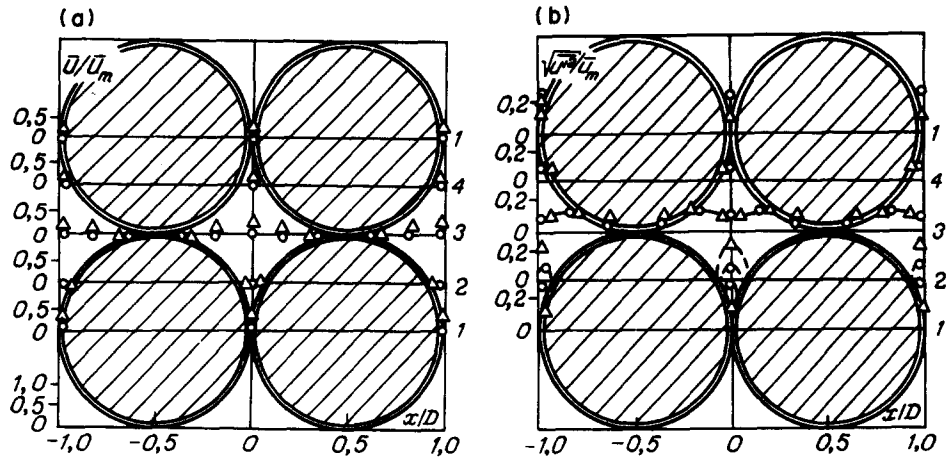

Figures 6(a, b). The same as figures 5(a, b) but at $y/D = 0.39$ and 0.44.

decreases from 1 in section 1 to 0.75 in section 2 and to 0.67 in section 3. Negative velocities up to $-0.15 \cdot \bar{u}_m$ are registered in the region of the wake contact points of beads at $r_1/D = \pm 1.0$. The turbulence level increases along the flow from ~11% in section 1 to ~14% in section 2 and to ~17% in section 3.

The cross-flow component of the velocity vector is close to zero in sections 1 and 3. The intensity of the cross-flow fluctuations is practically equal to that of the longitudinal ones. The data in figures 7(a, b) are those for the range $\mathrm{Re} = 5 \cdot 10^3$ to $1.74 \cdot 10^4$.

The effect of Re on the longitudinal velocity profiles is shown in figure 8. Here, the solid line is for the profiles shown in figure 3(a) for the near-wall and central cells at $\mathrm{Re} = 1.74 \cdot 10^4$.

The data points are experimental results using a cubic bed over the Re range $2.4 \cdot 10^2$ to $2.5 \cdot 10^3$, obtained by Volkov *et al.* (1980). It follows that, with increasing Re, the data points for the dimensionless velocities approximate those shown by the solid line. The longitudinal velocity profiles reach the asymptote for the filtrational flow quickest in the central cell. In the near-wall cell the process is slower. Negative velocities of $(0.1\text{–}0.2) \cdot \bar{u}_m$ in the reverse flow area are registered over the whole Re range from $2.4 \cdot 10^2$ to $2 \cdot 10^4$.

Experimental data for the cross-flow and transverse components of the velocity vector in the filtrational flow at $\mathrm{Re} = 1.74 \cdot 10^4$ (central cell) are shown in figures 9(a, b) and 10(a, b). In section $1(h/D = 0)$ in figure 9(a), the solid line indicates, for comparison, the longitudinal velocity profile. The cross-flow velocity, $\bar{v}/\bar{u}_m$, is close to zero in the jet core and increases smoothly up to $0.2 \cdot \bar{u}_m$ in the peripheral cell part in the region near the contact points. The transverse velocity, $\bar{w}/\bar{u}_m$, is also zero, due to the flow symmetry, in the jet core; in the peripheral cell it eventually reaches $0.15 \cdot \bar{u}_m$.

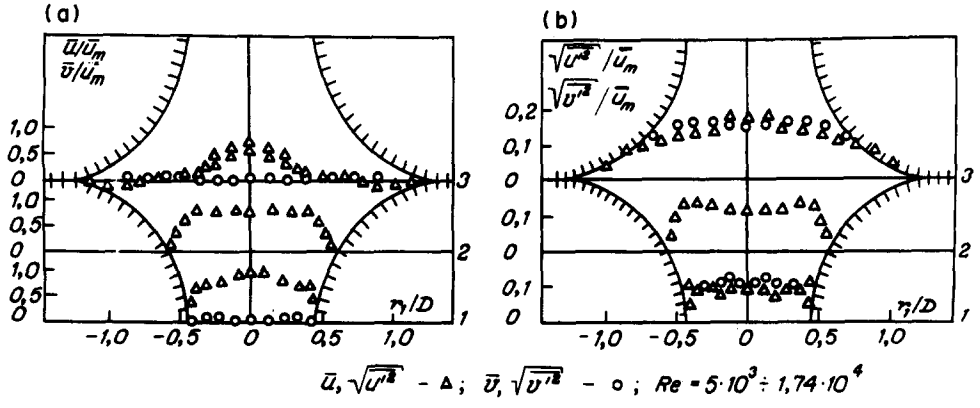

Figures 7(a, b). Longitudinal velocity profiles (a) and turbulent fluctuation levels (b) in a cubic cell at $\mathrm{Re} = 1.74 \cdot 10^4$ in the zr_1 symmetry plane.

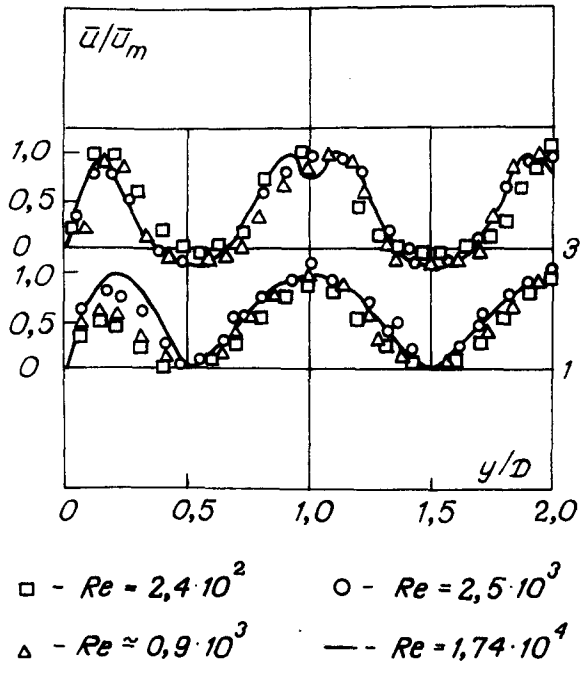

Figure 8. Effect of Re upon the longitudinal velocity in a cubic cell in a minimum and a maximum section.

The turbulence level in the jet part of the flow is ~9%; the intensities of all three components of the velocity vector are nearly the same. The exception is a region in close proximity to the bead contact points (at a distance of ~1 mm), where longitudinal fluctuations reach their maximum value of 24%.

In section 3 ($h/D = 0.5$) in figure 10(a), the cross-flow velocity is zero, while the transverse velocity changes within the range $(0.1\text{–}0.2)\cdot\bar{u}_m$. The turbulence maximum of ~18% in section 3 is located near the inflection points of the longitudinal velocity profile at $y/D = 0.75$ and 1.25. In the jet core it is ~14% and in the cell periphery, ~12%. The fluctuations of the three velocity components are practically the same. Compared with section 1, the intensity of the fluctuations has increased more than 1.5-fold.

The spectral characteristics of the turbulent velocity fluctuations have been studied at most typical flow points. Typical results are presented in figure 11, showing the spectral distribution of the energy of the fluctuations at the cell symmetry axis in the jet core (○) and in the transition region between the jet and the reverse flow, where the longitudinal velocity fluctuations are a maximum (●). The measurements were performed in the central cell plane 2, where the flow is

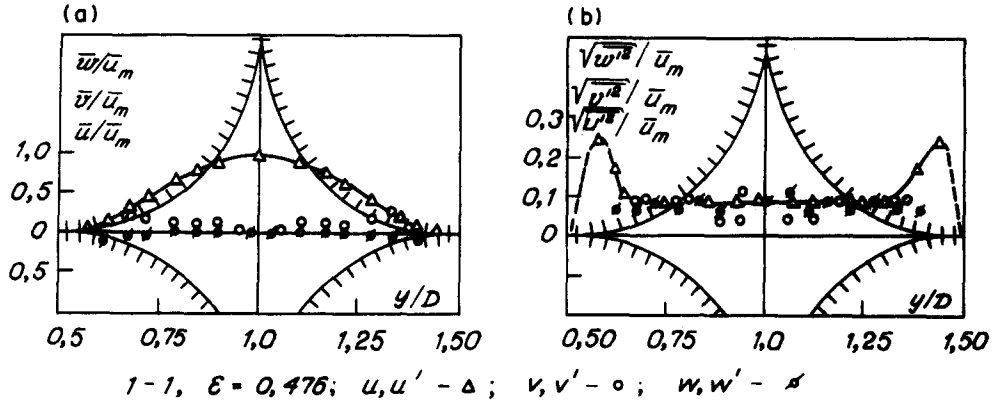

Figures 9(a, b). Profiles for the cross-flow and transverse components of the velocity vector (a) and for their r.m.s. fluctuations (b) in a cubic cell at $\mathrm{Re} = 1.74\cdot10^4$ in a minimum section.

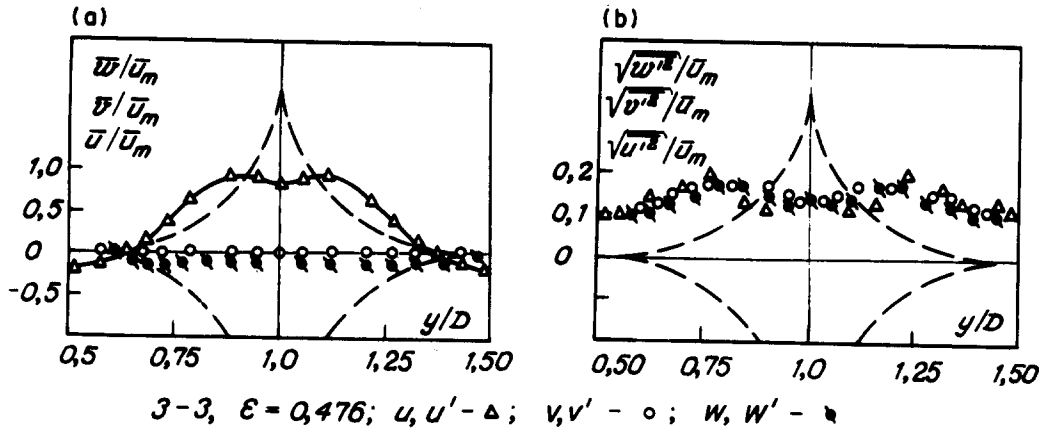

Figures 10(a, b). The same as figures 9(a, b) in a maximum section of a cubic cell.

expanding. The abscissa is $f \cdot D/\bar{u}_m$—the local Strouhal number defined at the quotient of the wavenumber K and $2\pi/D$ [f is the fluctuation frequency (Hz)]. The ordinate is the normalized energy of the velocity fluctuation $\phi \cdot \bar{u}_m/\overline{u'^2}D$, where $\overline{u'^2}$ is the energy in a broad frequency band and $\phi = (\overline{u'^2})_f/\Delta f$ is the energy density in the frequency band.

The spectral function has its maximum value, as is usual, at the minimum frequency measured (5 Hz). With increasing frequency, the spectral function decreases inversely with the square of the wavenumber. The spectral function decrease at medium frequencies differs from the known law of "$-5/3$" of Kolmogorov, Geyzenberg & Vaitszekker. It should be noted that there are no discrete

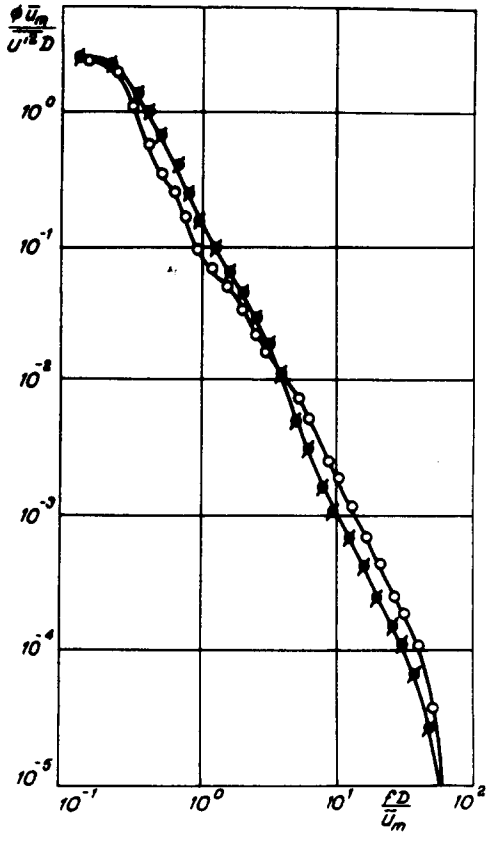

Figure 11. Spectra of the longitudinal velocity fluctuations in a cubic cell at the jet axis (○) and at a maximum of the fluctuations (●) at $\mathrm{Re} = 1.74 \cdot 10^4$.

components in the velocity fluctuation spectrum and that the highest fluctuations are of the order of a bead diameter.

4. FILTRATION PROCESSES IN AN OCTAHEDRIC PACKED BED

Flow in both octahedric and cubic packed beds is in the form of a rhomb with concave sides. Longitudinal channels are thereby blocked by beads, having 12 contact points between them.

Downstream inside a $0.706D$ high bead cell, there are two regions with a maximum passage for the flow at $h/D = 0.2$ and 0.5 [figure 1(a)]. The ratio of the maximum flow area to the minimum one is 1.6279. The filtration process inside a bead cell of an octahedric packed bed may be represented schematically as follows. A jet flowing toward and near a bead comes from section 1–1; it is formed by four jets in section 0–0 and after flowing around a bead it is divided into four jets again in section 2–2 [figure 1(c)]. The flow area in sections 0–0, 1–1 and 2–2 of a cell is minimal and each of the sections contains four bead contact points.

To construct a maximally close octahedric packed bed with constant porosity, the bead halves were placed near the walls and bead quarters—in the corners of the channel. During visual studies Re values were in the range 10^3 to $2 \cdot 10^4$.

The pattern of flow within the layer in an octahedric packed bed is displayed in figure 12(a) for Re = 1000. The beads are streamlined and show separation, only in the zone (about 0.1 cm in size) behind the contact points of the beads. In figure 12(b) the left-hand bead in the cell is lowered by 1 mm. The deformation of the bead in the cell is lowered by 1 mm. The deformation of the bead packing results in a significant increase in the size of the separation zone. As compared to a cubic packed bed, the free space between beads decreases sharply. The through channels of the flowing section of the cell are changed into blocked ones. The number of contact points of the beads increases by a factor of two. The flow geometry in section 1–1 ($h/D \simeq 0.35$) is identical to section 1 of the cubic bed. Figures 13(a, b) show distributions of the three components of the velocity vector and profiles for their r.m.s. fluctuations. In contrast to that in the cubic bed, the profile of the longitudinal velocity has two maxima equal to 1, located symmetrically relative to the cell longitudinal symmetry axis. In the cell centre, the flow velocity is $\sim 0.5\, u_m$. When Re increases from 10^3 to $2 \cdot 10^4$, the local maxima of the velocity profile move closer to the contact points, from the coordinate $y/D \simeq \pm 0.3$ to $y/D \simeq \pm 0.4$. The $\bar{v}$ cross-flow component of the velocity vector in the central part of the cell is zero at $y/D \simeq \pm 0.25$. It gradually decreases to minus $(0.02\text{–}0.05) \cdot \bar{u}_m$ near the bead contact points, i.e. fluid flows towards the bead contact points. The transverse component $\bar{w}$ changes smoothly from zero at the cell centre to approx. $-0.3 \cdot \bar{u}_m$ at $y/D \simeq \pm 0.4$, and then decreases to zero at the bead contact points ($y/D = \pm 0.5$). Practically the same profile for $\bar{w}$ is observed in the cubic arrangement.

Longitudinal velocity fluctuation intensities near the bead contact points are similar in both arrangements, so that their profiles in the region from $y/D = \pm 0.5$ to $y/D \simeq \pm 0.4$ nearly coincide. But in the central part of cell, longitudinal fluctuations are ~ 2.5 times higher in an octahedric arrangement than in a cubic one, i.e. $\sim 20\%$ on average. With Re increasing from 10^3 to $2 \cdot 10^4$, the turbulence level in the section considered increases, on average, from 10 to 20%, but in the central part of the cell it is practically constant and equals $\sim 20\%$. The intensity of the v and w fluctuations in the central part from $y/D = 0$ to $y/D \simeq \pm 0.3$ is similar to that of the longitudinal component. Close to the bead contact points there is a decrease in the v and w fluctuations down to zero. The fluctuations of v and w in a cubic bed are 2–3 times smaller than in an octahedric one.

The profile of the longitudinal velocity in a direction at an angle of 45° to the x-axis is similar to that for a turbulent regime of flow in a channel. The velocity gradient is a maximum at the bead walls. Longitudinal fluctuations through the section do not exceed $\sim 16\%$ and undergo little change through the whole Re range under investigation. Maxima in the fluctuating velocity are found only

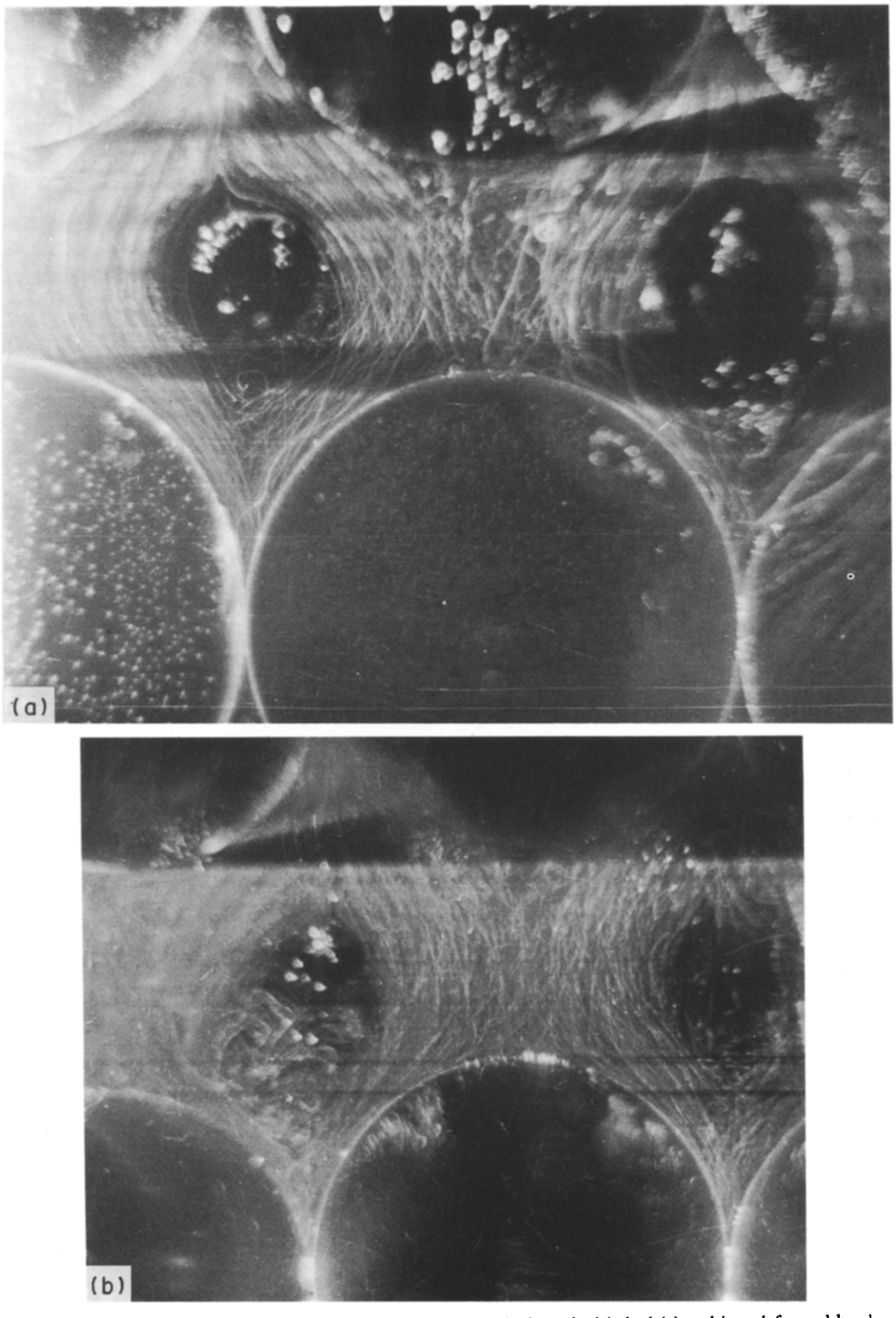

Figures 12(a,b). Turbulent filtrational flow in a close packed octahedric bed (a) and in a deformed bead cell (b) at Re = 1000.

in the vicinity of the bead walls. They are equal to ~22% and are apparently associated with turbulence generated by the bead walls (surface).

In the ~1.5 mm gap between the beads in the r_2-direction (section 1–1), the longitudinal velocity profile has a bell-like shape with a maximum of $(0.82–0.85)\cdot u_m$ located at the symmetry axis.

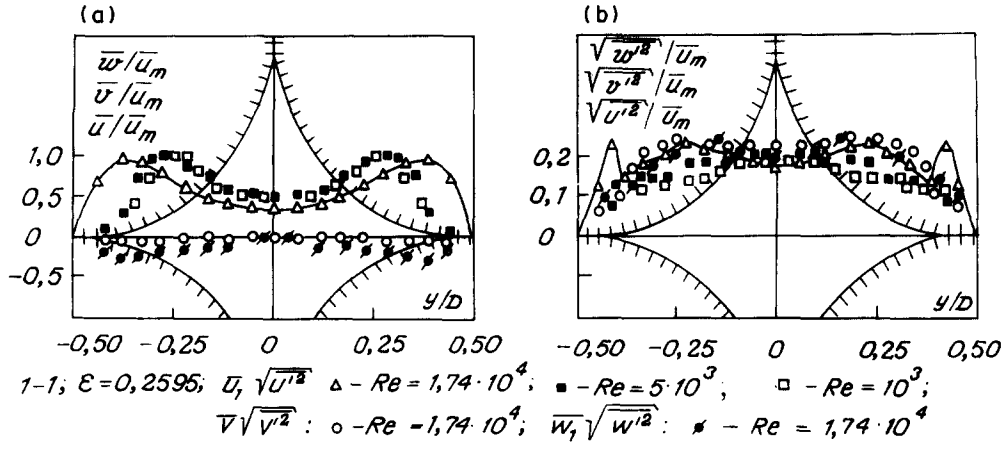

Figures 13(a, b). Profiles for the three velocity vector components (a) and their r.m.s. fluctuations (b) in an octahedric cell at $Re = 10^3$ to $2 \cdot 10^4$ (minimum section 1–1).

Maxima of the longitudinal velocity fluctuations are about 20% and are located at a distance of 0.2 mm from the bead surface in the turbulence generation zone. The level of velocity fluctuations in the gap is ~18%.

As stated previously, the flow in section 1–1 of the octahedric cell is formed by four jets formed, in turn, downstream in section 0–0; then, in section 2–2, the fluid flows around the bead and is again divided into four jets. So we may assume that the filtrational flow properties of sections 0–0 and 2–2 are similar ($h/D = 0$ and 0.706). Moreover, the parameters of each of the four jets in both sections 0–0 and 2–2 must be similar, in accordance with the symmetry conditions.

The profiles of the longitudinal and transverse velocities, as well as those of their r.m.s. fluctuations, in cell section 0–0 are shown in figures 14(a, b). Here the symmetry axis r of the jet section is at an angle of 45° to the y-axis, in accordance with the flowing part of the cell. The maxima, equal to 1.0, shift towards the contact points of the spheres, and the velocity minimum on the symmetry axis of the cell varies from 0.75 to 0.55.

Cross-flow velocity profiles in sections 1–1 and 0–0 differ significantly. The local maximum of the cross-flow velocity is located at the symmetry axis of the jet section and is $\sim 0.25\ \bar{u}_m$. In approaching a bead contact point, the cross-flow velocity $\bar{v}$ changes its sign, reaches the value of $-0.35 \cdot \bar{u}_m$ at a distance of ~1.8 mm from the contact point and decreases to zero at the bead contact point.

The mean level of fluctuations in the longitudinal velocity in sections 0–0 is ~18%. Cross-flow fluctuations are also evenly distributed over the section at a level of ~14%. Local maxima of the longitudinal velocity fluctuations at a distance of 1.4–2.0 mm from the bead contact points are 24–28%.

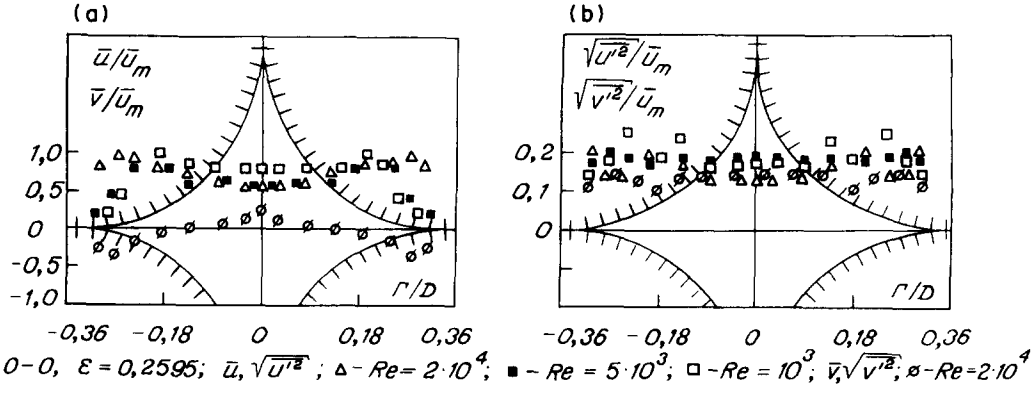

Figures 14(a, b). Profiles for the longitudinal and cross-flow velocities (a) and their r.m.s. fluctuations (b) in an octahedric cell at $Re = 10^3$ to $2 \cdot 10^4$ (minimum section 0–0).

The longitudinal velocity profile is of a bell-like form in the direction of the r^*-symmetry axis, being at an angle of 45° to the r-axis. The velocity fluctuations are uniformly distributed over the section and are at a level of about 18%. In the vicinity of the bead surface, maxima of the velocity fluctuations are 25–27% and are apparently associated with turbulence generation by this surface.

Spectral characteristics of the turbulent fluctuations at a point on the symmetry axis in section 1–1 are given in figure 15 for three Re values: 10^3, $5 \cdot 10^3$ and $2 \cdot 10^4$. The coordinates of the diagram are the same as in figures 14(a, b): the local Strouhal number $f \cdot D/\bar{u}_m$ is along the x-axis, and the y-axis is the normalized energy of the velocity fluctuations $\phi \cdot \bar{u}_m/u'^2 \cdot D$. Spectra were measured in the frequency range 25–1000 Hz. The investigation has shown that with increasing frequency, the spectral function decreases inversely with the square of wavenumber K, as in a cubic arrangement. This means that the spatial correlation function of longitudinal fluctuations is exponential, i.e. there is a variety of vortices in the flow with sizes varying from the order of a bead diameter to the dissipative size.

5. DISCUSSION

Visual studies and detailed measurements of the local flow structure inside the pores support the hypothesis of a jet-like character of the flow through a packed bed suggested by Gol'dshtik (1984). In a cubic arrangement, flow separation increases up to $\sim 150°$, i.e. separation phenomena occur in an area close to the wake contact points of the beads. Four local separation areas are also formed inside a cubic cell behind each lateral contact point, which are connected in a complicated way in the wake (separation) part of the bead. Profiles for the longitudinal velocity in the wakes in section $3(h/D = 0.5)$ of a cubic cell are shown in figures 16(a,b) for $y/D = 0.055$ to 0.44. The projection of zero velocity lines in the wake gives, as shown in figure 17, a separation area in the wake that is depicted by the solid circle, and a reverse flow zone behind the contact points, depicted by the dashed curves. The flow pattern inside the cubic bead cell, in our opinion, agrees well with the flow pattern of a liquid in immediate proximity to a bead surface presented by Karabelas *et al.* (1973) for streamline flow through a single layer of beads.

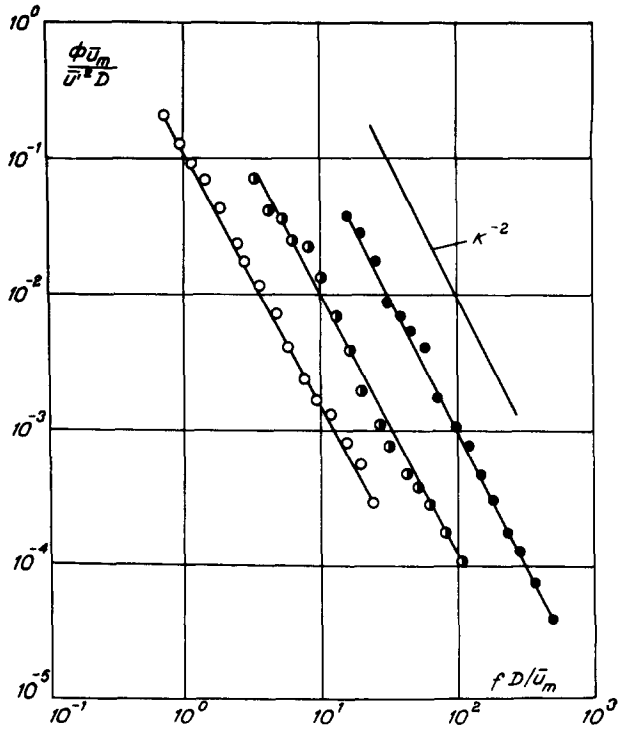

Figure 15. Spectra of the longitudinal velocity fluctuations in an octahedric cell at the symmetry axis at $Re = 10^3$ to $2 \cdot 10^4$ (minimum section 1–1).

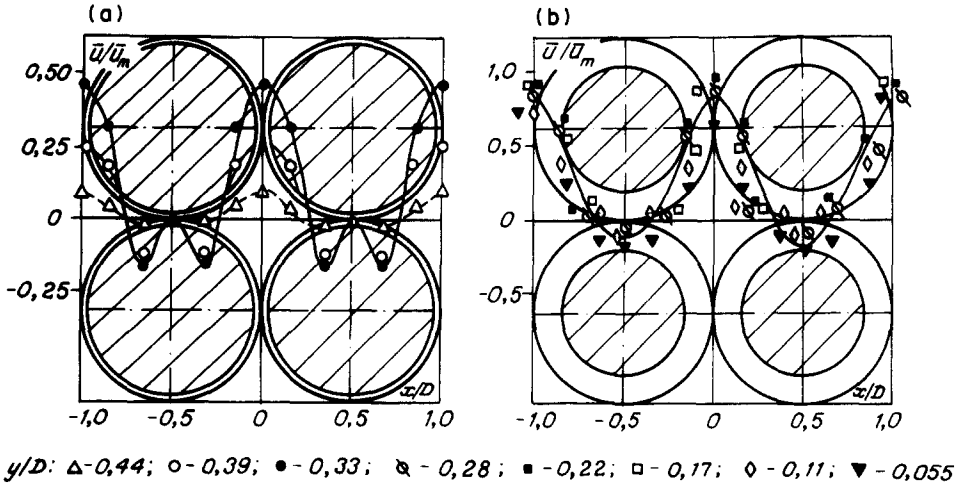

Figures 16(a, b). Longitudinal velocity profiles in the shadow bead area ($h/D = 0.5$) in a cubic cell at $y/D = 0.055$ to 0.44 ($\mathrm{Re} = 1.74 \cdot 10^4$).

Local separation areas are observed behind the bead contact points only in visual studies which are analogous to those described by Wegner *et al.* (1971) and Karabelas *et al.* (1973) for a rhombohedric arrangement. They are significantly smaller in size than the bead diameter ($\sim 0.1D$). These areas are difficult to measure. Longitudinal velocity profiles show no separation in any of the octahedric cell sections that were investigated. But the turbulence level of filtrational flow inside an octahedric cell is 2–2.5 times higher than that inside a cubic cell at similar Re. The above discrepancies result mainly from differences in the geometry of the cells. A significant decrease in octahedric cell volume due to the blocking of a through passage by a bead leads to a significant decrease in local separation areas behind the contact points of the beads. On the other hand, the very turbulent jet near the bead in the cell is formed by four jets downstream and is then split into four jets again. This process plays a leading role in turbulence generation inside an octahedric cell and in maintaining the high level of turbulence in the jets.

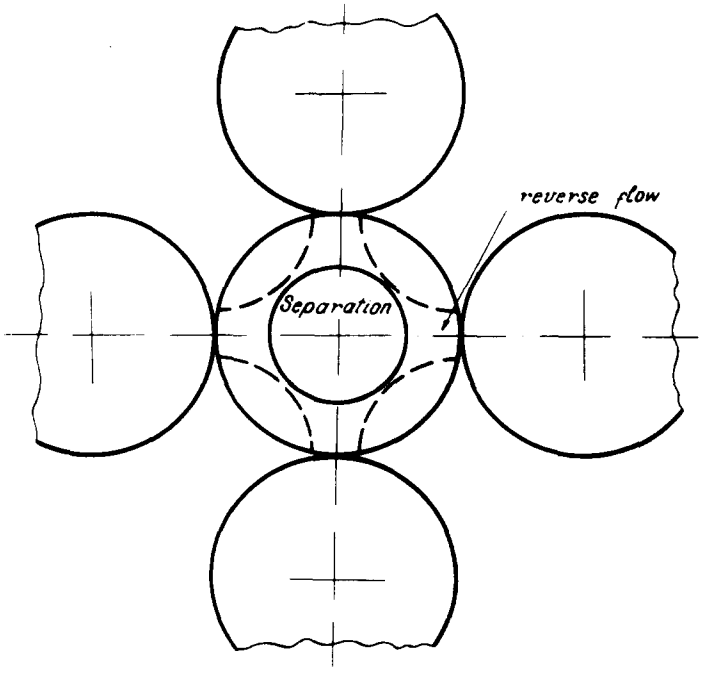

Figure 17. Projection of separation areas on to the shadow bead area in a cubic cell.

The turbulence generation mechanism in a cubic cell is associated primarily with the interaction of jets and separation areas. The turbulence level in their mixing layer is found to be the same as that inside an octahedric cell.

6. CONCLUSIONS

Visual studies and detailed measurements of the local structure of flow inside the pores in cubic and dense octahedral cells in the Re range from 10^3 to $2 \cdot 10^4$ were performed.

Local flow separations from the bead walls behind the points of contact with neighbouring beads are found. In a cubic cell the length of the separation zone downstream amounts to $\sim(0.6–0.7)D$ and the cross size is $(0.3–0.4)D$. In the wake region these local separations merge in a similar way to that represented in the model of flow past a single layer of beads presented by Karabelas *et al.* (1973). In the octahedral dense bead cell the zones of flow separation behind the points of bead contact are analogous to those given in the model by Wegner *et al.* (1971) and have sizes of $\sim 0.1D$.

The mechanism of turbulence generation in the cells is not similar. In the octahedric cell it is associated with the process of joining and separation of jets in accordance with the geometry of the channels with flowing fluid; in the cubic cell—with interaction between a jet and separation areas, in the mixing layer of which the turbulence level amounts to $\sim 24\%$.

Fluctuations in the three components of the velocity vector are practically the same for both types of beds. The average turbulence level in jets in the octahedric bed is 20%. In the cubic cell, it increases along the jet from ~ 10 to $\sim 15\%$.

By analysing the distribution of the r.m.s. fluctuations in each cell considered, it was found that the turbulence generation near the bead surface does not influence the integral value of turbulence energy in a cell. The bead surfaces orient the flow and influence flow turbulence indirectly, through the adhesion condition. The contact points of the beads and their associated separation phenomena are of great significance in forming the turbulent filtrational flow structure at high Re.

REFERENCES

AEROV, M. E. & TODES, O. N. 1968 *Gidravlicheskiye i Teplovye Osnovy Raboty Apparatov so Statsionarnym i Kipyashchim Zernistym Sloem*, p. 510. Himiya, Leningrad (in Russian).

AEROV, M. E., TODES, O. N. & NARINSKII, D. A. 1972 *Apparaty Sostatsionarnym Zernistym Sloem*, p. 176. Himiya, Leningrad (in Russian).

BERNARD, J., WANG, C. & LEE, R. 1981 Measurement of fluid velocities in the interior of the transparent fluidized bed with a laser-Doppler anemometer. *AIChE Symp. Ser.* **77**(205), 37–50.

BOGOYAVLENSKII, R. G. 1978 *Gidrodinamika i Teploobmen v Vysokotemperaturnyh Yadernyh Reaktorah a Sharovymi Tvelami*, p. 112. Atomizdat, Moscow (in Russian).

BORISHANSKII, V. M. 1958 Soprotivleniye pri dvizhenii vozduha cherez sloi sharov—V kn.: TsKTI im. Polzunova. *Voprosy Aerodinamiki i Teploperedachi v Kotelno-topochnyh Protsessah*, p. 70. Gosenergoizdat, Moscow (in Russian).

GOL'DSHTIK, M. A. 1984 *Protsessi Perenosa v Zernistom Sloe*, p. 163. Nauka/Institut teplofiziki SO AN SSSR, Moscow/Novosibirsk (in Russian).

JOHNSTON, W., DYBBS, A. & EDWARDS, R. 1975 Measurement of fluid velocity inside porous media with a laser anemometer. *Phys. Fluids* **18,** 813–914.

JOLLS, K. R. & HANRATTY, T. J. 1966 Transition to turbulence for flow through a dumped bed of spheres. *Chem. Engng Sci.* **21,** 1185–1190.

KARABELAS, A. S., WEGNER, T. H. & HANRATTY, T. J. 1973 Flow pattern in a close packed cubic array of spheres near the critical Reynolds number. *Chem. Engng Sci.* **28,** 673.

KIRILLOV, V. A., MATROS, Yu. Sh., SOROKIN, V. N., KASAMANYAN, M. A. & SLINKO, M. G. 1972 Gidrodinamicheskaya obstanovka v svobodnom objeme sloya katalizatora. *Dokl. Akad. Nauk SSSR* **206,** 1409–1411 (in Russian).

VOLKOV, V. I. 1980 Issledovaniya gidrodinamiki i protsessov perenosa v poristyh sredah, p. 166. Kand. Diss., Instituta teplofiziki SO AN SSSR, Novosibirsk (in Russian).

VOLKOV, V. I., DANILOV, N. S., ZHAK, V. D., NAKORYAKOV, V. E. 1980 Investigation of near-wall layer hydrodynamics using cubic arrangement model. *Zh. Prikl. Mekh. tekh. Fiz.* **6,** 58.

WEGNER, T. H., KARABELAS, A. S. & Hanratty, T. J. 1971 Visual studies of flow in a regular array of spheres. *Chem. Engng Sci.* **26,** 59.

YEVSEYEV, A. R. & RYASHENTSEVA Ye. S. 1986 Ghidkost dlya opticheskih issledovanii. Report A. s. 1204623 SSSR, M. kl.^{3} C. 09.K3/00 (in Russian).